# Обзор ArXiv/astro-ph, 13-18 апреля 2018 года

От Сильченко О.К.

# Astro-ph: 1804.05853

## The EDGE-CALIFA Survey: Molecular and Ionized Gas Kinematics in Nearby Galaxies


Rebecca C. Levy,[1] Alberto D. Bolatto,[1] Peter Teuben,[1] Sebastián F. Sánchez,[2] Jorge K. Barrera-Ballesteros,[3] Leo Blitz,[4] Dario Colombo,[5] Rubén García-Benito,[6] Rodrigo Herrera-Camus,[7] Bernd Husemann,[8] Veselina Kalinova,[5] Tian Lan,[9,10] Gigi Y. C. Leung,[8] Damián Mast,[11,12] Dyas Utomo,[4,13] Glenn van de Ven,[8,14] Stuart N. Vogel,[1] and Tony Wong[9]

[1]*Department of Astronomy, University of Maryland, College Park, MD 20742, USA*

[2]*Instituto de Astronomía, Universidad Nacional Autónoma de México, A.P. 70-264, 04510 México, D.F., Mexico*

[3]*Department of Physics & Astronomy, Johns Hopkins University, Baltimore, MD 21218, USA*

[4]*Department of Astronomy, University of California, Berkeley, CA 94720, USA*

[5]*Max-Planck-Institut für Radioastronomie, D-53121, Bonn, Germany*

[6]*Instituto de Astrofísica de Andalucía, CSIC, E-18008 Granada, Spain*

[7]*Max-Planck-Institut für Extraterrestrische Physik, D-85741 Garching bei Müchan, Germany*

[8]*Max-Planck-Institut für Astronomie, Königstuhl 17, D-69117 Heidelberg, Germany*

[9]*Department of Astronomy, University of Illinois, Urbana, IL 61801, USA*

[10]*Department of Astronomy, Columbia University, New York, NY 10027, USA*

[11]*Universidad Nacional de Córdoba, Observatorio Astronómico de Córdoba, Córdoba, Argentina*

[12]*Consejo de Investigaciones Científicas y Técnicas de la República Argentina, C1033AAJ, CABA, Argentina*

[13]*Department of Astronomy, The Ohio State University, Columbus, OH 43210, USA*

[14]*European Southern Observatory (ESO), 85748 Garching bei München, Germany*



### ABSTRACT

We present a comparative study of molecular and ionized gas kinematics in nearby galaxies. These results are based on observations from the EDGE survey, which measured spatially resolved $^{12}$CO(J=1–0) in 126 nearby galaxies. Every galaxy in EDGE has corresponding resolved ionized gas measurements from CALIFA. Using a sub-sample of 17 rotation

# Обзор молекулярного газа EDGE-CALIFA

### 2.1. *The EDGE-CALIFA Survey*

The EDGE-CALIFA survey (Bolatto et al. 2017) measured CO in 126 nearby galaxies with CARMA in the D and E configurations. Full details of the survey, data reduction, and masking techniques are discussed in Bolatto et al. (2017), and we present a brief overview here. The EDGE galaxies were selected from the CALIFA sample (discussed in the following section) based on their infrared (IR) brightness and are biased toward higher star formation rates (SFRs) (see Figure 6 of Bolatto et al. 2017). A pilot study of 177 galaxies was observed with the CARMA E-array. From this sample, 126 galaxies selected for CO brightness were re-observed in the D-array. These 126 galaxies with combined D and E array data constitute the main EDGE sample[1]. The EDGE sample is the largest sample of galaxies with spatially resolved CO, with typical angular resolution of 4.5″ (corresponding to ∼1.5 kpc at the mean distance of the sample). Data cubes were produced with 20 km s$^{-1}$ velocity channels. At each pixel in the cube, a Gaussian is fit to the CO line. Velocity-integrated intensity, mean velocity, velocity dispersion, and associated error maps are created from the Gaussian fits. Pix-

Of the 126 EDGE galaxies, ≈100 have peak brightness temperatures $\geq 5\sigma$ (Bolatto et al. 2017). Reliable CO and H$\alpha$ rotation curves could not, however, be derived for every detected EDGE galaxy. To best compare the CO and H$\alpha$ rotation curves, a sub-sample of galaxies for which reliable CO and H$\alpha$ rotation curves could be derived is used for the remainder of the analysis (the Kinematic Sub-Sample or KSS). A reliable rotation curve has small $V_{\rm rad}$ and $\Delta V_{\rm sys}$ components at radii larger than $R_{\rm 2beam}$ (as in Figure 3). In the centers of galaxies, there may be radial motions due to bars and other effects, but these should not affect the larger radii we consider here. Ensuring that both the CO and H$\alpha$ have small $V_{\rm rad}$ components validates our assumptions that the CO and H$\alpha$ have the same PA and inclination and that the PA and inclination do not change much over the disk (i.e. there are no twists or warps). In addition to the criteria on the rotation curves, there are four galaxies (NGC 4676A, NGC 6314, UGC 3973, and UGC 10205) for which the observed CO velocity width may not be fully contained in the band (Bolatto et al. 2017). One galaxy (UGC 10043) has a known H$\alpha$ outflow (López-Cobá et al. 2017). These galaxies are also excluded from the subsample. Finally, we exclude galaxies with inclinations larger than 75°. At large inclinations, the line profiles can become skewed and a Gaussian fit to the line profiles is not appropriate and can lead to systematic biases in the mean velocities. We do, however, plan to analyze the highly inclined galaxies in a forthcoming paper

**Осталось 17 галактик**

# Примеры полей скоростей

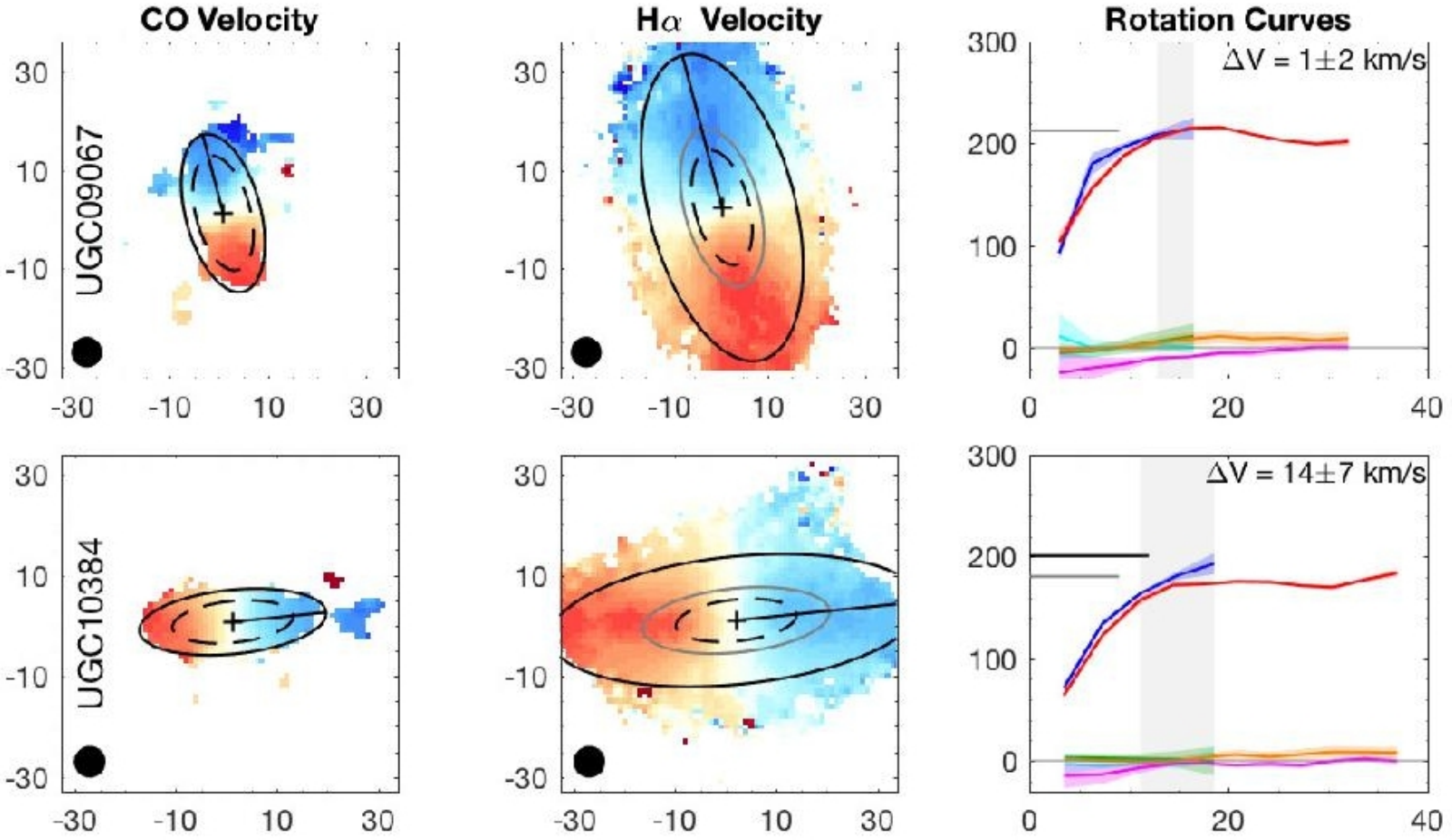

# Сравнение кривых вращения по эмиссиям и по CO

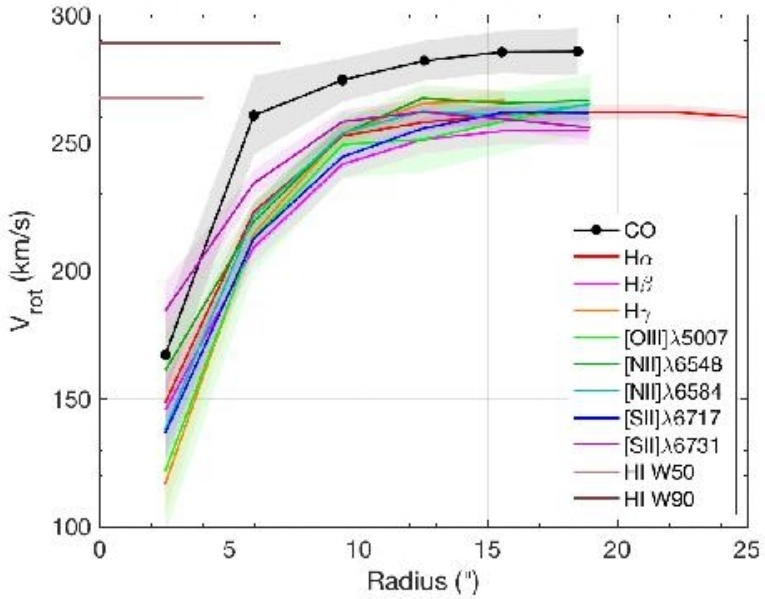


**Figure 6.** Rotation curves in several ionized gas lines are consistent with each other (using fixed geometric parameters listed in Table 4). The figure shows an example for NGC 2347. For CO, the shaded region shows the error on the rotation curves from variations in the kinematic parameters using the Monte Carlo method described in Section 3.1. For all other curves, the shaded regions indicate the formal errors from the rotation curve fitting. The rotation curves from the ionized gas are consistent with one another and are all below the CO rotation curve. Ionized rotation curves other than H$\alpha$ are truncated at the same radius as CO. The tan and brown horizontal lines show $V_{rot}$(HI) from W50 and W90 measurements, which tend to agree with the CO rotation velocity. Note that variations among the rotation curves are enhanced as the y-axis does not extend down to zero.

# У ранних типов ионизованный газ еще горячей

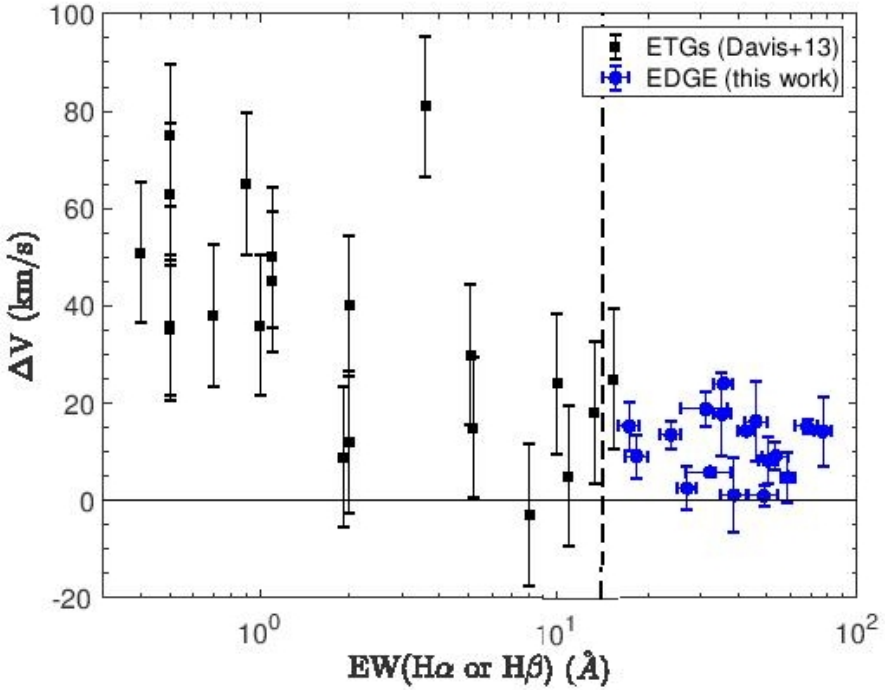


**Figure 7.** Equivalent width of the H$\alpha$ or H$\beta$ emission versus rotation velocity difference between the molecular and ionized gas, $\Delta V$. The blue points are the KSS galaxies and use EW(H$\alpha$), and the black points are ETGs from Davis et al. (2013) who use the luminosity weighted mean EW(H$\beta$), excluding those which are counter-rotating. Error bars are not provided for the EW(H$\beta$) data. Our points are consistent with the low $\Delta V$ end of the ETGs. EWs > 14 Å (vertical dashed line) trace star formation (Lacerda et al. 2018), so it is not surprising that the star-forming disk galaxies used in this study have larger EWs than the ETGs use by Davis et al. (2013).

# Вывод: в эмиссионных линиях наблюдается смесь тонкого диска и толстого диффузного.

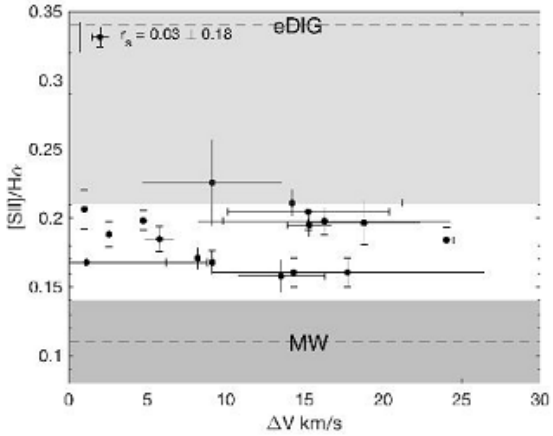


(a)

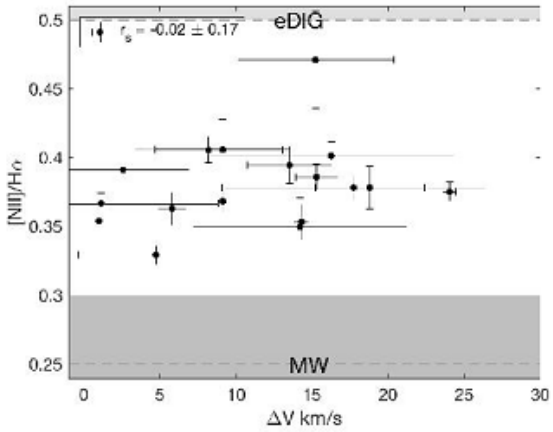


(b)

# Astro-ph: 1804.04470

## Galaxy and Mass Assembly (GAMA): Variation in Galaxy Structure Across the Green Valley

Lee S. Kelvin,[1] Malcolm N. Bremer,[2] Steven Phillipps,[2] Philip A. James,[1] Luke J. M. Davies,[3] Roberto De Propris,[4] Amanda J. Moffett,[5] Susan M. Percival,[1] Ivan K. Baldry,[1] Chris A. Collins,[1] Mehmet Alpaslan,[6] Joss Bland-Hawthorn,[7] Sarah Brough,[8] Michelle Cluver,[9] Simon P. Driver,[3,10] Abdolhosein Hashemizadeh,[3] Benne W. Holwerda,[11] Jarkko Laine,[12] Maritza A. Lara-Lopez,[13] Jochen Liske,[12] Witold Maciejewski,[1] Nicola R. Napolitano,[14] Samantha J. Penny,[15] Cristina C. Popescu,[16,17] Anne E. Sansom,[16] Will Sutherland,[18] Edward N. Taylor,[19] Eelco van Kampen[20] and Lingyu Wang[21,22]

# Взяли узкий диапазон масс

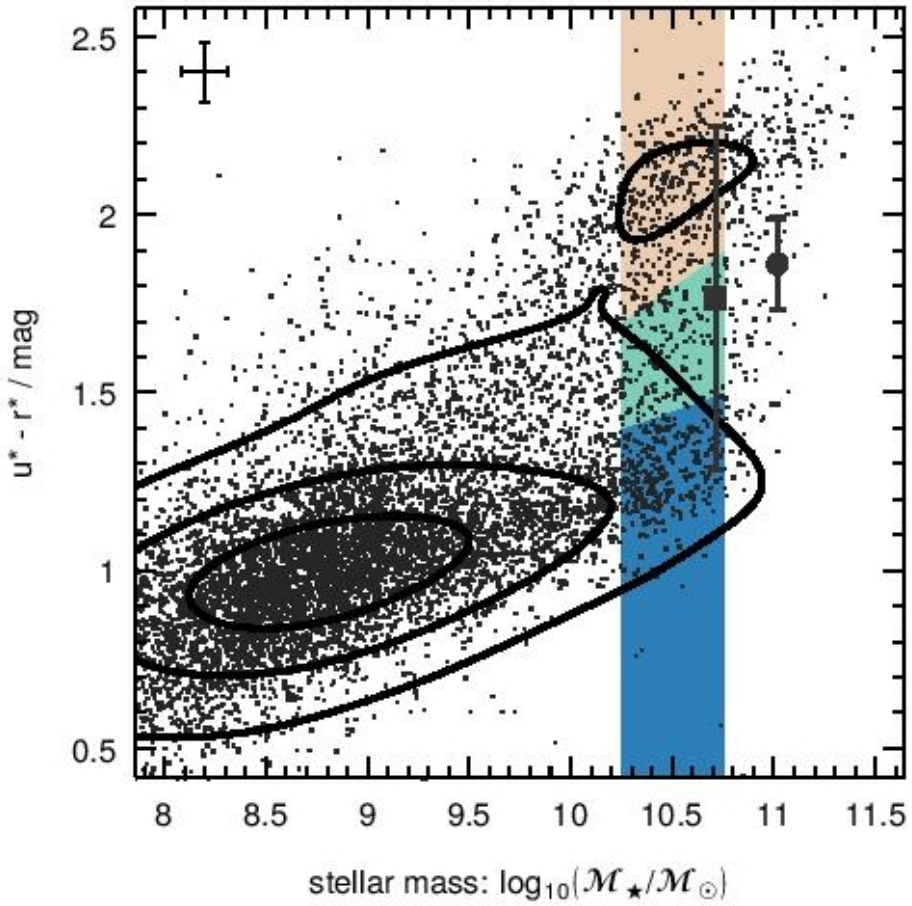

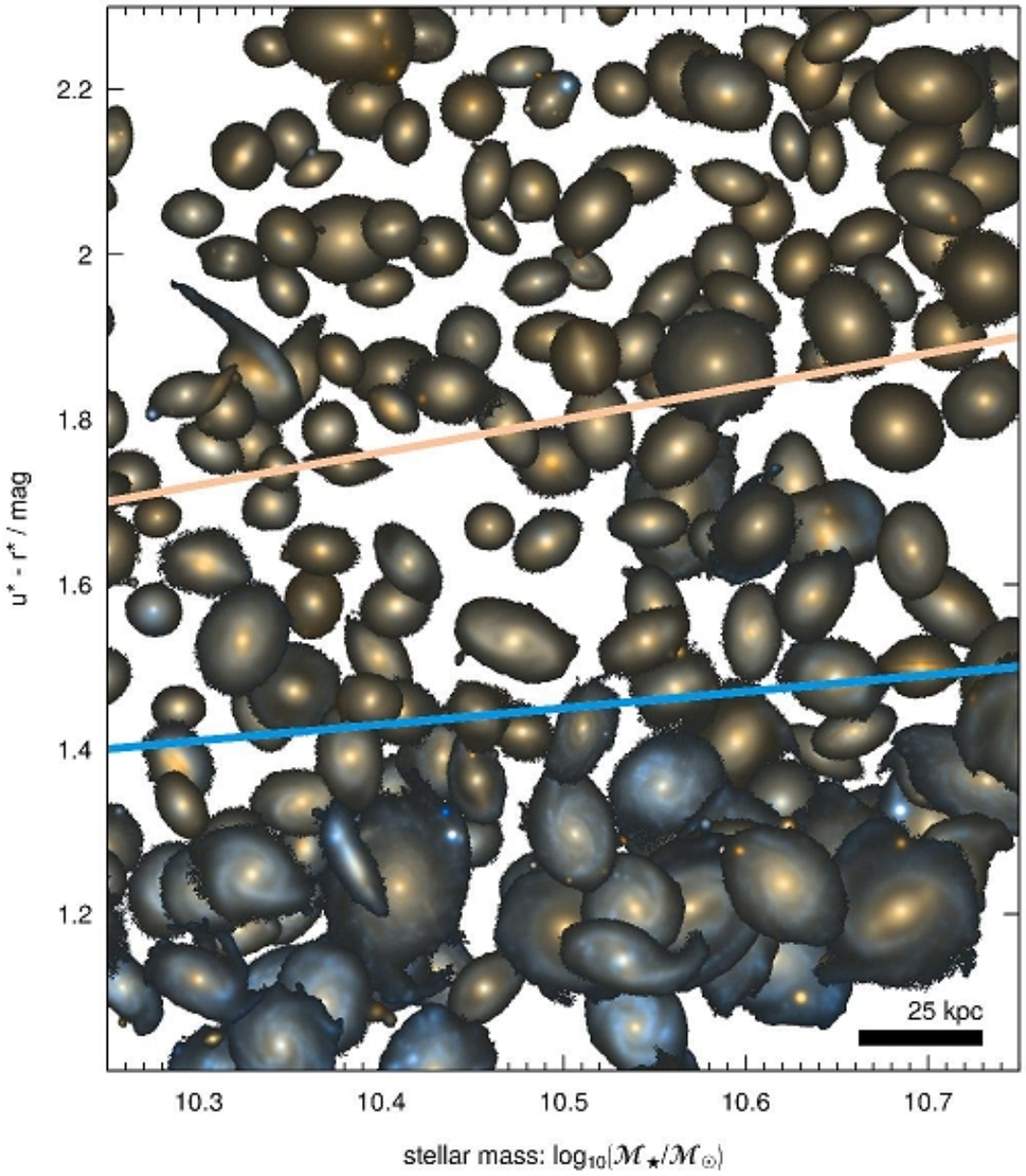


**Figure 3.** Postage stamps for 203 representative galaxies in our final sample. These false 3-colour galaxy images are based on KiDS $g$ and $r$ band imaging. Galaxies are located at their reference position in the colour–stellar-mass plane (cf. Figure 1). Solid red and blue lines indicate our chosen boundaries between the red, green and blue sub-populations. Images are scaled to physical units as represented by the inset legend.

# Ручная классификация деталей!

## 4 RESULTS

Results from our Green Valley Census are reduced into a final catalogue as follows. Based on the number of votes given by classifiers, each galaxy is assigned a score from 0 to 8 for each of the six structural indicators shown in Section 3, namely: bar, ring/partial ring, plateau/lens, tidal tails/streams, shell/shells and interaction/merger. Those galaxies with 4 or more votes in any given category are assigned to that category, i.e., at least half of the classifiers must have classified the galaxy in that way. Our elliptical population shows no significant trends for many of these structural markers, as might be expected, and therefore we limit our further analyses to disk-type galaxies alone (S0-Sa, Sab-Scd and Sd-Irr). This disk-type population is split by colour into red, green and blue sub-groups as discussed in Section 2.3. A vote fraction is determined for each sub group with fractional errors assigned following the beta distribution quantile technique (Cameron 2011). Errors derived in such a fashion are consistent with other techniques (e.g., normal approximation) when applied to large datasets, yet have been shown by Cameron (2011) to outperform such traditional methodologies for small data samples. Example galaxies meeting the above classification criteria for each of the six structural components are shown in Figure 4, with the final row providing examples for which none of the above structures were noted.

| Hubble Type | Red | | Green | | Blue | | Total | |
|---|---|---|---|---|---|---|---|---|
| E | 87 | | 27 | | 10 | | 124 | |
| S0-Sa | 121 | | 51 | | 56 | | 228 | |
| Sab-Scd | 3 | 126 | 11 | 62 | 103 | 160 | 117 | 348 |
| Sd-Irr | 2 | | 0 | | 1 | | 3 | |
| Total | 213 | | 89 | | 170 | | 472 | |

**Table 1.** Breakdown by Hubble type and colour for all 472 galaxies in our final sample. Braces show total numbers for disk-type galaxies (S0-Sa, Sab-Scd and Sd-Irr).

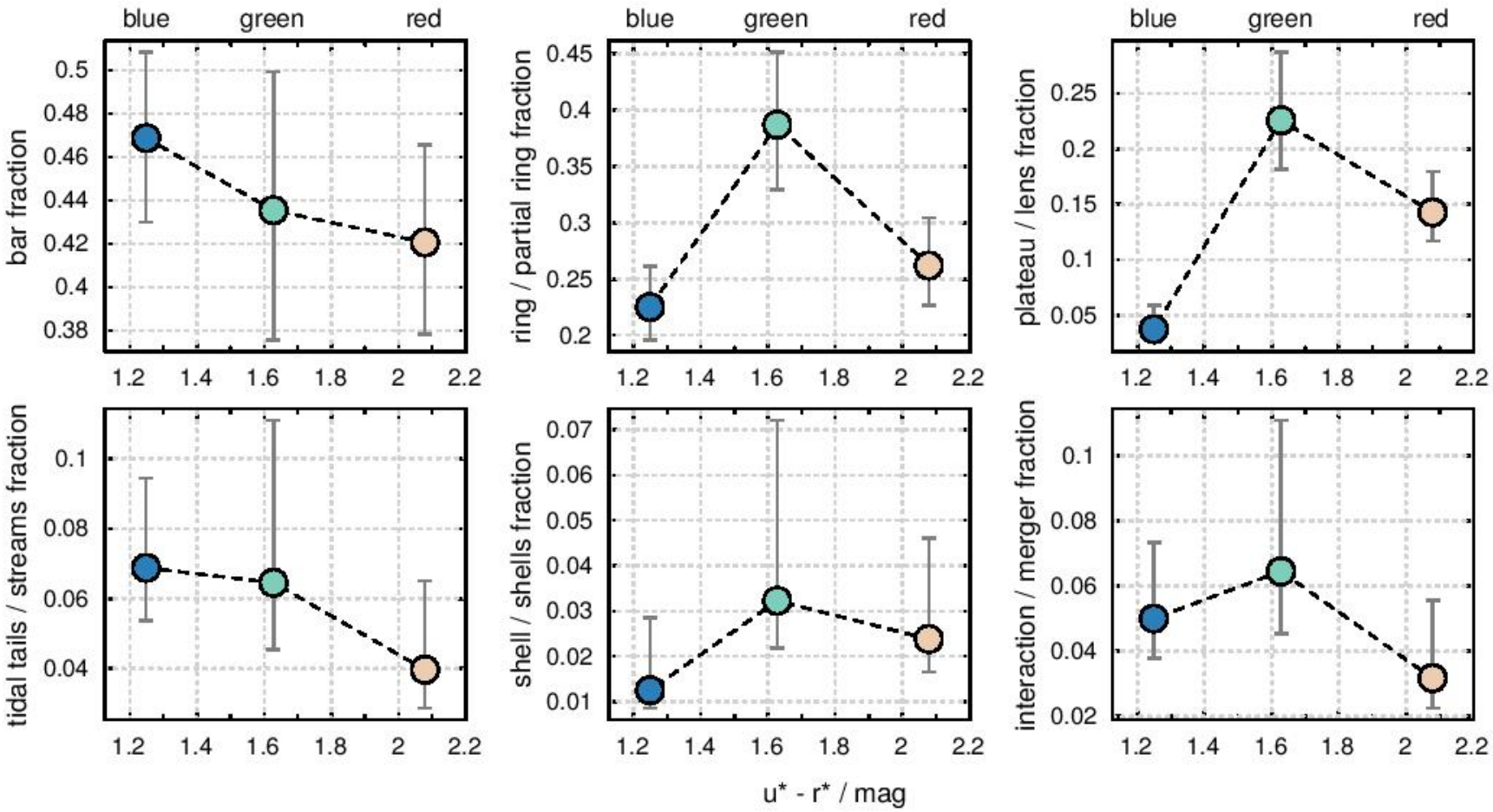
blue
green
red
bar fraction
0.5
0.48
0.46
0.44
0.42
0.4
0.38
ring / partial ring fraction
0.45
0.4
0.35
0.3
0.25
0.2
plateau / lens fraction
0.25
0.2
0.15
0.1
0.05
tidal tails / streams fraction
0.1
0.08
0.06
0.04
shell / shells fraction
0.07
0.06
0.05
0.04
0.03
0.02
0.01
interaction / merger fraction
0.1
0.08
0.06
0.04
0.02
1.2
1.4
1.6
1.8
2
2.2
u* - r* / mag

# В зеленой долине - значимый избыток колец и линз

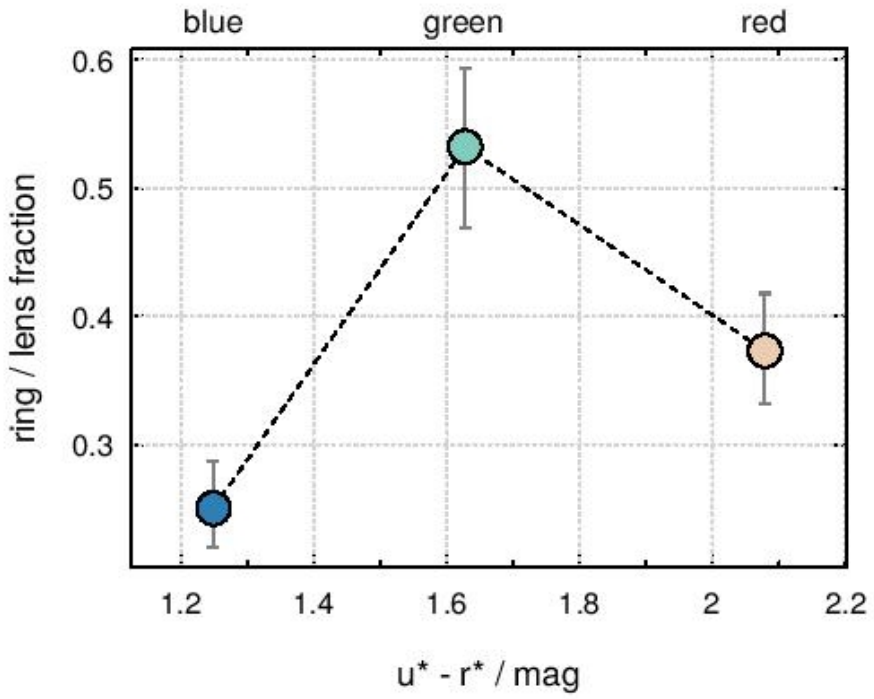


**Figure 7.** Number fraction for recovered ring/lens type structures as a function of $u^* - r^*$ colour for disk-type galaxies. Error bars represent $1\sigma$ confidence intervals.

# В барных галактиках всего больше, НО… параллельно!

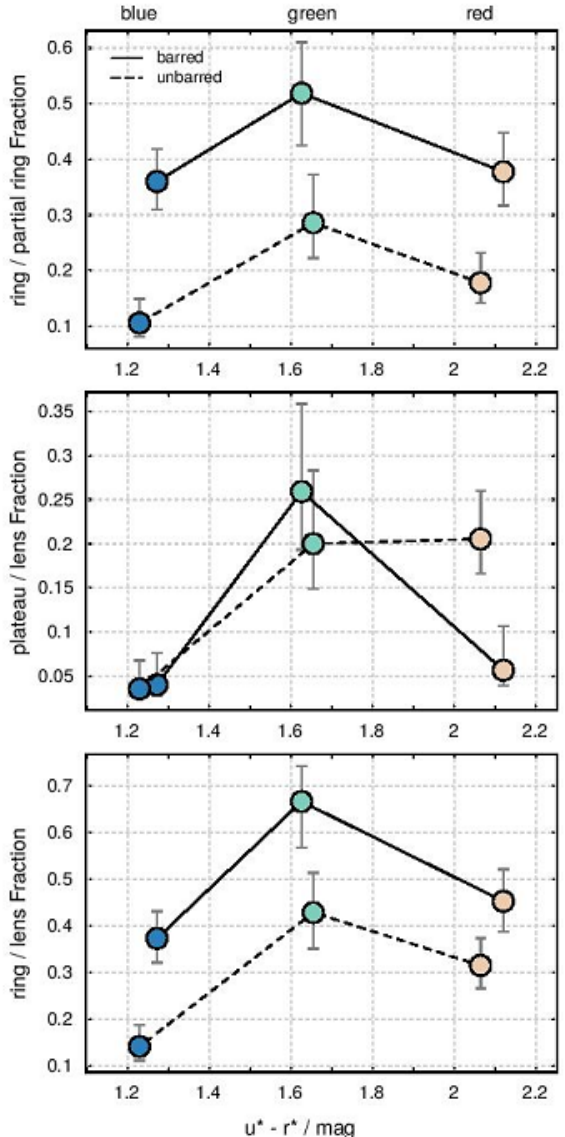

# Astro-ph: 1804.04663

## The angular momentum-mass relation: a fundamental law from dwarf irregulars to massive spirals

Lorenzo Posti[1,⋆], Filippo Fraternali[1], Enrico M. Di Teodoro[2] and Gabriele Pezzulli[3]

[1] Kapteyn Astronomical Institute, University of Groningen, P.O. Box 800, 9700 AV Groningen, the Netherlands
[2] Research School of Astronomy and Astrophysics - The Australian National University, Canberra, ACT, 2611, Australia
[3] Department of Physics, ETH Zurich, Wolfgang-Pauli-Strasse 27, 8093 Zurich, Switzerland

Received XXX; accepted YYY

**ABSTRACT**

In a ΛCDM Universe, the specific stellar angular momentum ($j_*$) and stellar mass ($M_*$) of a galaxy are correlated as a consequence of the scaling existing for dark matter haloes ($j_\mathrm{h} \propto M_\mathrm{h}^{2/3}$). The shape of this law is crucial to test galaxy formation models, which are currently discrepant especially at the lowest masses, allowing to constrain fundamental parameters, e.g. the retained fraction of angular momentum. In this study, we accurately determine the empirical $j_* - M_*$ relation (Fall relation) for 92 nearby spiral galaxies (from S0 to Irr) selected from the *Spitzer* Photometry and Accurate Rotation Curves (SPARC) sample in the unprecedented mass range $7 \lesssim \log M_*/M_\odot \lesssim 11.5$. We significantly improve all previous estimates of the Fall relation by determining $j_*$ profiles homogeneously for all galaxies, using extended HI rotation curves, and selecting only galaxies for which a robust $j_*$ could be measured (converged $j_*(< R)$ radial profile). We find the relation to be well described by a single, unbroken power-law $j_* \propto M_*^\alpha$ over the entire mass range, with $\alpha = 0.55 \pm 0.02$ and orthogonal intrinsic scatter of $0.17 \pm 0.01$ dex. We finally discuss some implications for galaxy formation models of this fundamental scaling law and, in particular, the fact that it excludes models in which discs of all masses retain the same fraction of the halo angular momentum.

# Профиль специфического момента: кривая вращения по HI, профиль плотности по S4G

### 3. The specific angular momentum-mass relation

If a galaxy is axisymmetric and rotates on cylinders about its symmetry axis, then the *specific stellar angular momentum* $j_* \equiv |\mathbf{J}_*|/M_*$ within the radius $R$ from the galactic centre writes as

$$j_*(<R) = \frac{\int_0^R \mathrm{d}R'\ R'^2\,\Sigma_*(R')\,V_{*,\mathrm{rot}}(R')}{\int_0^R \mathrm{d}R'\ R'\,\Sigma_*(R')}, \qquad (1)$$

where $\Sigma_*(R) = \Upsilon_{\mathrm{b}}^{[3.6]}\,I_{\mathrm{b}}(R) + \Upsilon_{\mathrm{d}}^{[3.6]}\,I_{\mathrm{d}}(R)$ is the surface stellar mass density, with $I_{\mathrm{b}}$ and $I_{\mathrm{d}}$ being the surface brightnesses of the bulge/disc at 3.6 $\mu$m, and $V_{*,\mathrm{rot}}$ the stellar rotation curve. The total specific stellar angular momentum is $j_* \equiv j_*(<R_{\mathrm{max}})$, where $R_{\mathrm{max}}$ is the outermost radius at which $\Sigma_*$ is measured. We compute the galaxy stellar mass as $M_* = 2\pi \int_0^{R_{\mathrm{max}}} \mathrm{d}R'\,R'\Sigma_*(R')$.

# Примеры радиальных распределений специфического момента

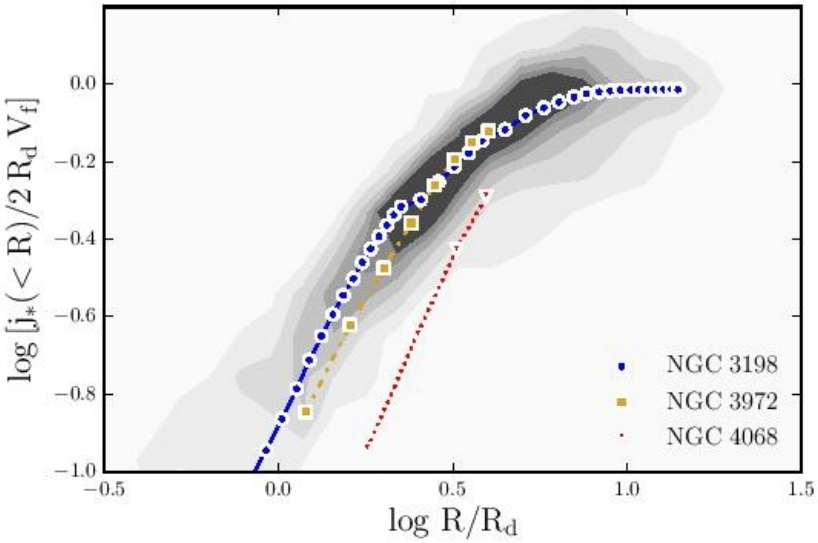


**Fig. 1.** Stellar specific angular momentum profiles for 175 disc galaxies in the SPARC sample. Grey contours represent the distribution of all the points in the profile of each galaxy. The radius is normalised to the disc scale length ($R_d$ at 3.6 $\mu$m) and $j_*$ to that of a thin exponential disc with the same $R_d$ and with a constant rotation curve. We also show the full profiles for three representative galaxies in our initial sample: a galaxy with a fully converged $j_*(< R)$ profile (blue circles), a galaxy with a converging profile (yellow squares) and a galaxy with a non-converging profile (red triangles). For our determination of the Fall relation, we excluded galaxies with a non-converging profile.

To further illustrate our selection, we highlight in Fig. 1 the individual $j_*$ profiles of three galaxies in the SPARC sample, representative of different converging properties. NGC 3198 has a perfectly converged $j_*$ profile (blue circles). In our sample, 28 galaxies, covering the entire SPARC mass range, show a similar feature: these are the galaxies for which $j_*$ is best measured. NGC 3972 (yellow squares) is the archetype of the galaxies that merely comply to the criteria of Eq. 2; these galaxies have a converging $j_*$ profile and the difference between the last two points of the profile is smaller than 10%. NGC 4068 (red triangles) has a steeply rising $j_*$ profile that does not meet Eq. 2 criteria; 34 similar galaxies are excluded from the calibration of the local Fall relation since their total $j_*$ might be severely underestimated.

# Главный результат: связь момента со звездного массой (диска) галактики

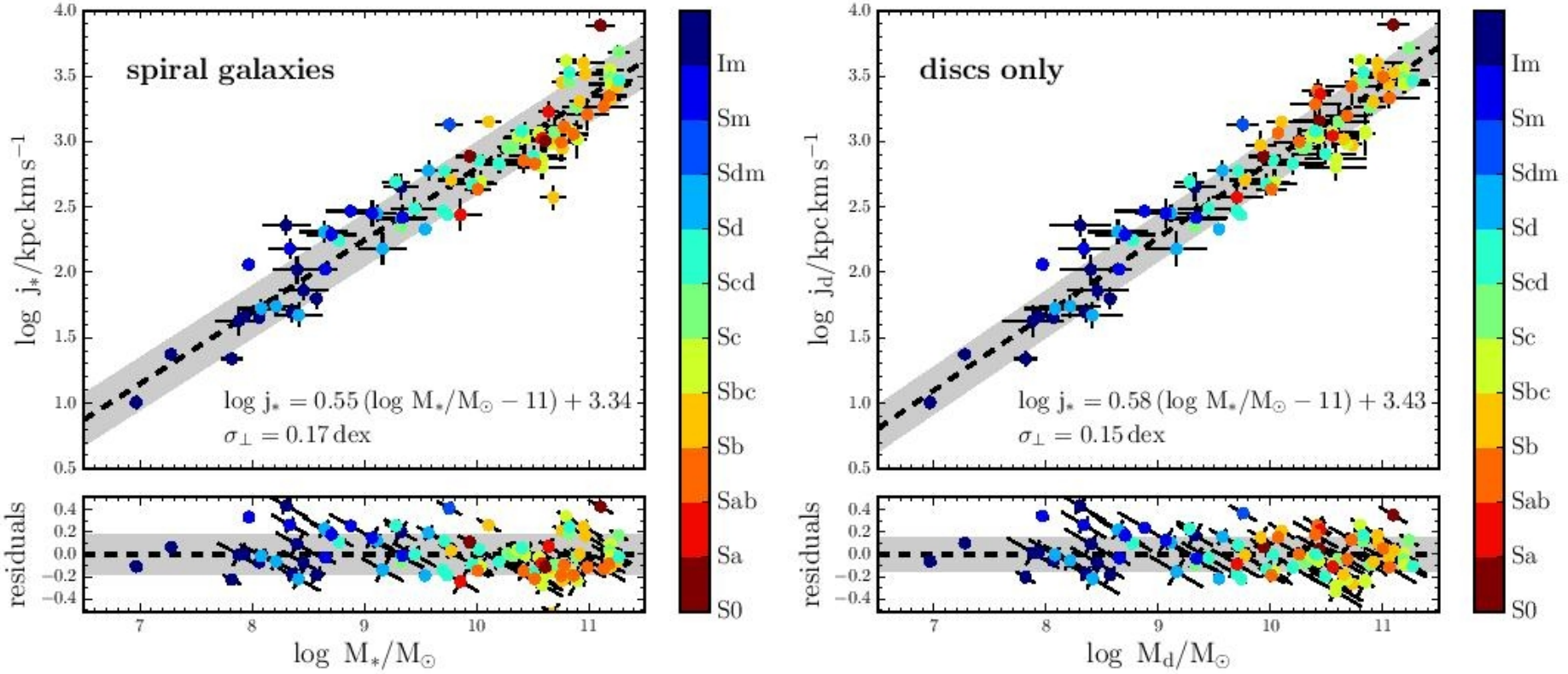


**Fig. 2.** *Left-hand panel:* specific stellar angular momentum-stellar mass relation (Fall relation) for a sample of 92 nearby disc galaxy. Each galaxy is represented by a circle coloured by Hubble type. The black dashed line is the best-fitting linear model and the grey band is the $1\sigma$ orthogonal intrinsic scatter. The bottom panel shows the orthogonal residuals around the linear model. *Right-hand panel:* same as the left-hand panel, but for the discs only (i.e. after removing the contribution from the bulges).

# Сравнение с моделями – в пользу `biased star formation' (предпочтение формированию звезд из низкомоментного газа)

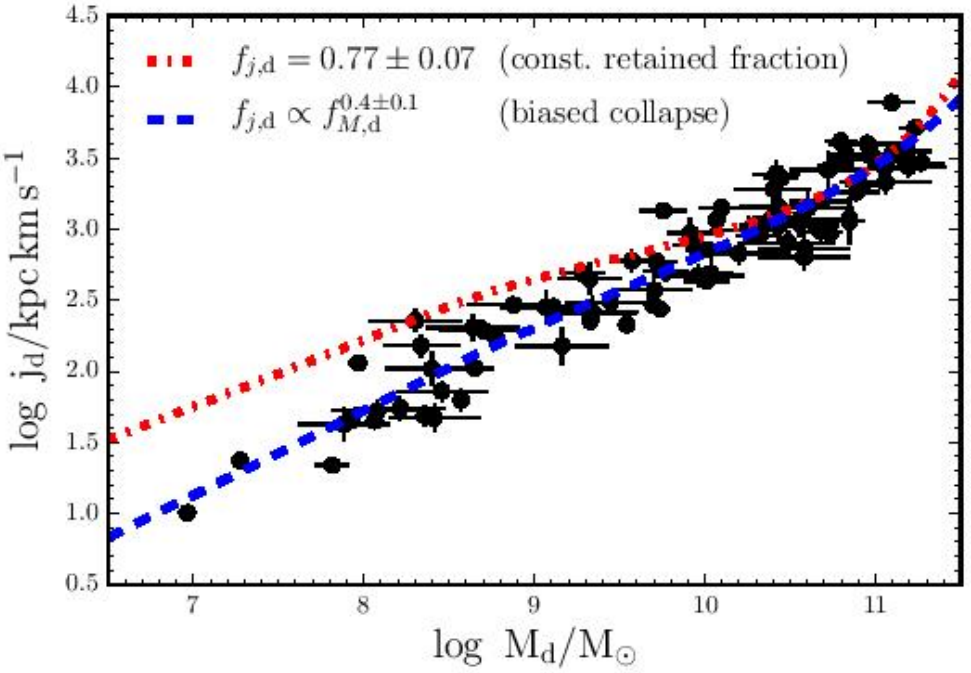


**Fig. 3.** Predicted distribution in the $j_\mathrm{d} - M_\mathrm{d}$ plane of a model with a constant retained fraction of angular momentum $f_j$ (red dot-dashed line) and for a *biased collapse* model (blue dashed line) compared to the data as in Fig. 2. To compute the two models we have used the stellar-to-halo mass relation from Rodríguez-Puebla et al. (2015).